Geophysical Research Letters

RESEARCH LETTER
10.1029/2018GL079286

Key Points:
- A method is developed to constrain aerosol vertical profiles in the boundary layer using hyperspectral measurements of oxygen absorption
- The method is tested using hyperspectral measurement of reflected solar radiation from a mountaintop instrument to infer aerosol profiles
- The method can potentially be applied to satellite observations to constrain aerosol vertical structure on a global scale

Supporting Information:
- Supporting Information S1

Correspondence to:
Z.-C. Zeng,
zcz@gps.caltech.edu

Citation:
Zeng, Z.-C., Natraj, V., Xu, F., Pongetti, T. J., Shia, R.-L., Kort, E. A., et al. (2018). Constraining aerosol vertical profile in the boundary layer using hyperspectral measurements of oxygen absorption. *Geophysical Research Letters*, *45*. https://doi.org/10.1029/2018GL079286

Received 20 JUN 2018
Accepted 23 SEP 2018
Accepted article online 27 SEP 2018

Constraining Aerosol Vertical Profile in the Boundary Layer Using Hyperspectral Measurements of Oxygen Absorption

Zhao-Cheng Zeng[1], Vijay Natraj[2], Feng Xu[2], Thomas J. Pongetti[2], Run-Lie Shia[1], Eric A. Kort[3], Geoffrey C. Toon[2], Stanley P. Sander[2], and Yuk L. Yung[1,2]

[1]Division of Geological and Planetary Sciences, California Institute of Technology, Pasadena, CA, USA, [2]Jet Propulsion Laboratory, California Institute of Technology, Pasadena, CA, USA, [3]Department of Climate and Space Sciences and Engineering, University of Michigan, Ann Arbor, MI, USA

Abstract This study attempts to infer aerosol vertical structure in the urban boundary layer using passive hyperspectral measurements. A spectral sorting technique is developed to retrieve total aerosol optical depth (AOD) and effective aerosol layer height (ALH) from hyperspectral measurements in the 1.27-μm oxygen absorption band by the mountaintop Fourier Transform Spectrometer at the California Laboratory for Atmospheric Remote Sensing instrument (1,673 m above sea level) overlooking the LA basin. Comparison to AOD measurements from Aerosol Robotic Network and aerosol backscatter profile measurements from a Mini MicroPulse Lidar shows agreement, with coefficients of determination (r^2) of 0.74 for AOD and 0.57 for effective ALH. On average, the AOD retrieval has an error of 24.9% and root-mean-square error of 0.013, while the effective ALH retrieval has an error of 7.8% and root-mean-square error of 67.01 m. The proposed method can potentially be applied to existing and future satellite missions with hyperspectral oxygen measurements to constrain aerosol vertical distribution on a global scale.

Plain Language Summary Satellite and ground-based measurements have enabled accurate and continuous monitoring of total aerosol loading. However, these measurements provide little or no information on the vertical distribution of aerosols. In particular, there is poor measurement of aerosols in the planetary boundary layer, the part of the atmosphere closest to the surface. In this study, we develop an algorithm to retrieve the vertical structure of aerosols in the boundary layer using remote sensing observations of oxygen absorption with high spectral resolution. The algorithm is applied to infer the vertical profile of air pollutants in the Los Angeles basin using measurements made by a mountaintop instrument overlooking the basin. The proposed retrieval algorithm can potentially be applied to existing and future satellite missions with hyperspectral oxygen measurements to constrain the aerosol vertical distribution on a global scale. This important piece of information on aerosol vertical structure will potentially address several key priorities in the 2017 U.S. National Research Council Earth Science Decadal Survey, from forecasting air pollution in cities, quantifying the aerosol impact on Earth's climate, and reducing biases in greenhouse gas retrievals.

1. Introduction

Information about the global abundance, properties, and height distribution of aerosols is needed to quantify their influence on the Earth's climate and to better validate climate models, (Intergovernmental Panel on Climate Change, 2013). In addition, the health effects from pollution are the largest environmental risk (Liu & Diner, 2017). Aerosols also affect greenhouse gas retrievals from space by influencing the path of atmospheric radiation (see, e.g., Butz et al., 2009; Kuang et al., 2002; O'Dell et al., 2012). Aerosols also affect fluorescence retrievals performed in O_2 absorption bands (Frankenberg et al., 2011). Aerosols, including those that contribute to poor air quality, are produced primarily within the planetary boundary layer (PBL), which is the bottom layer of the atmosphere and couples the Earth's surface and the atmosphere above. However, this near-surface layer is relatively poorly modeled, including the air pollutants trapped within this mixing layer. Improving our understanding of the PBL processes is critical to model the coupling mechanisms between the atmosphere and land in the integrated Earth system. Moreover, more accurate representation of the PBL processes related to aerosol horizontal and vertical distributions and composition can improve modeling of cloud formation and atmospheric radiative transfer (RT; Zarzycki & Bond, 2010).

Column measurements of aerosol optical depth (AOD) have been accurately and continuously observed by satellites such as Moderate Resolution Imaging Spectroradiometer (Kahn et al., 2007) and Multiangle Imaging Spectroradiometer (Diner et al., 1998) and by ground-based measurements from Aerosol Robotic Network (AERONET; Holben et al., 1998). These measurements provide little or no information on the vertical distribution of aerosols. Lidar measurements (Winker et al., 2009) have proven helpful in providing information that locates aerosol layers using active remote sensing. However, lidar instruments have a narrow swath, and it is therefore very difficult to obtain a global coverage. It has long been recognized that passive remote sensing using absorption spectroscopy of molecular oxygen has the potential for aerosol vertical profiling (Hou et al., 2017; Yamamoto & Wark, 1961). Absorption in the center of strong O_2 lines is saturated, such that any radiance measured in these regions must originate from scattering in the upper part of the atmosphere. In weak lines light can penetrate to lower atmospheric layers, allowing for the quantification of aerosols and other scatterers near the surface. This passive technique has been used to study cloud top height and cloud thickness (Heidinger & Stephens, 2000; O'Brien & Mitchell, 1992; Richardson et al., 2017; Yamamoto & Wark, 1961) and to investigate its potential for aerosol profiling using theoretical studies (Colosimo et al., 2016; Davis et al., 2017; Gabella et al., 1999; Geddes & Bösch, 2015; Hollstein & Fischer, 2014; Timofeyev et al., 1995) and broadband oxygen measurements from Scanning Imaging Absorption Spectrometer for Atmospheric Chartography (Sanghavi et al., 2012), Deep Space Climate Observatory (DSCOVR) (F. Xu, van Harten, et al., 2017; X. Xu, Wang, et al., 2017), POLarization and Directionality of the Earth's Reflectances (POLDER), and Medium Resolution Imaging Spectrometer (MERIS) (Dubuisson et al., 2009). In addition, satellite and airborne measurements in the ultraviolet may have the potential to retrieve the absorbing aerosol layer height (ALH; Torres et al., 1998; F. Xu, van Harten, et al., 2017; X. Xu, Wang, et al., 2017). Model simulations have shown that spectrally resolved (hereafter referred to as hyperspectral) measurements in O_2 absorption bands have, in principle, sufficient information content for quantifying the aerosol vertical distribution and its optical and microphysical properties (Hou et al., 2017). However, very limited progress has been made using real measurements. Aerosol profiling within the boundary layer is even more challenging because resolving the aerosol profile at subkilometer scales requires accurate hyperspectral measurements, good knowledge of aerosol optical properties and compositions, and correct characterization of surface reflection.

In this study, an algorithm based on a spectral sorting technique is proposed to retrieve the total AOD and the effective ALH in the boundary layer using hyperspectral measurements in the oxygen band centered at 1.27 μm. The algorithm is applied to measurements made by the Fourier Transform Spectrometer at the California Laboratory for Atmospheric Remote Sensing (CLARS-FTS), located on the top of Mt. Wilson (1,673 m above sea level) overlooking the LA basin.

2. Data

2.1. Observations From CLARS

The CLARS-FTS instrument is located on the top of Mt. Wilson (1,673 m above sea level) in the LA basin and offers continuous high-resolution spectral measurements in the near infrared to shortwave infrared spectral region (effectively from 4,000 to 12,000 cm^{-1}), including the oxygen $^1\Delta$ band at 1.27 μm. As shown in Figure S1 in the supporting information, CLARS has two modes of operation: the Spectralon Viewing Observation mode, which quantifies the solar irradiance by measuring reflected sunlight from a Spectralon plate located immediately below the FTS telescope, and the Los Angeles Basin Survey mode, which measures reflected sunlight from surface targets in the basin. In this study, we focus on the West Pasadena surface target, as illustrated in Figure S2a. The CLARS observation geometry makes the measurements not only highly sensitive to the atmospheric composition but also very susceptible to influence by aerosol scattering and absorption due to the long light path across the boundary layer. The CLARS measurements mimic to a certain extent the off-nadir viewing of an instrument in geostationary orbit with hourly viewing capability. Details concerning the CLARS-FTS design, operation, and calibration can be found in Fu et al. (2014), K. W. Wong et al. (2015), C. K. Wong et al. (2016), and Zeng et al. (2017). High and low clouds are filtered from the CLARS data using the oxygen ratio approach (K. W. Wong et al., 2015). This study does not require the CLARS spectra to be radiometrically calibrated since only the CLARS level reflectance (the ratio of the Los Angeles Basin Survey and Spectralon Viewing Observation radiances) is used, as shown in Figure S1b.

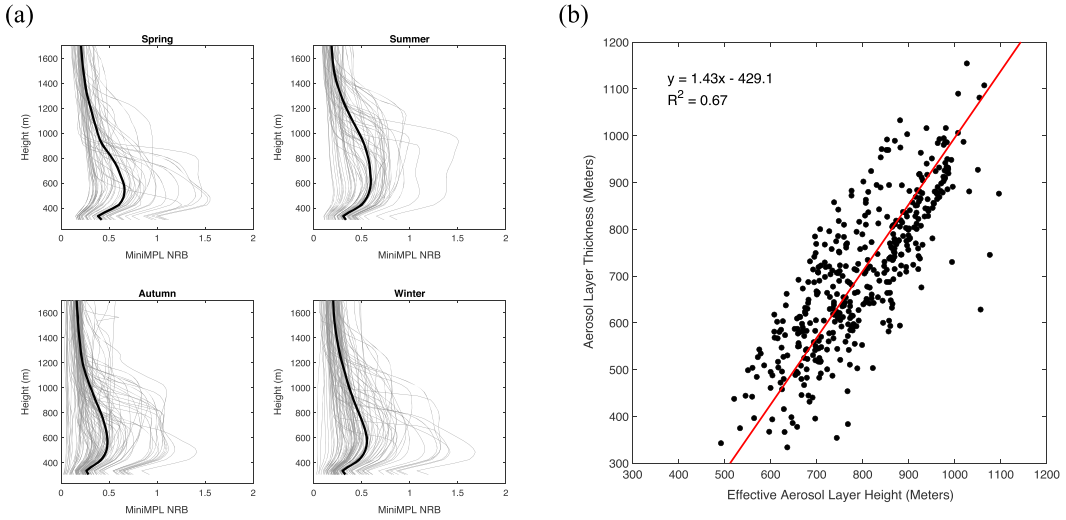

Figure 1. (a) Seasonal mean and variabilities of vertical profiles of normalized relative backscatter (NRB) at 2:00 p.m. measured by MiniMPL located at Caltech. The gray lines are all the available measurements from 2012 to 2014, and the bold black lines are the seasonal means. (b) Correlation between effective aerosol layer height and geometric thickness calculated using the MiniMPL measurements as shown in (a). The two parameters have a significant correlation (r^2 = 0.67). MiniMLP = Mini MicroPulse Lidar.

2.2. AERONET AOD Measurements

The AERONET site at Caltech makes measurements of total AOD, from which aerosol optical properties including single scattering albedo (SSA) and phase function can be retrieved. Text S1 introduces the estimation of AOD value in the O_2 $^1\Delta$ band at 1.27 μm using the Ångström exponent law. Figure S3 shows the seasonal histograms of AOD, SSA, and asymmetry parameter from the aerosol scattering phase function obtained from AERONET-Caltech from 2011 to 2017.

2.3. MiniMPL Aerosol Backscatter Measurements

The Mini MicroPulse Lidar (MiniMPL) instrument, located at Caltech, measures the aerosol backscattering at different altitudes by emitting 532-nm laser light and determining the distance to scattering events using the time of light travel (Ware et al., 2016). The raw event count reported by the MiniMPL at a vertical resolution of 30 m must be calibrated and normalized in order to arrive at the quantity of interest, viz, normalized relative backscatter (NRB), which is approximately proportional to the concentration of scatterers at a given distance above the instrument. Measurement data from 2012 to 2014 are used in this study. Figure 1a shows the seasonal mean and variabilities of vertical profiles of NRB at 2:00 p.m. The aerosol layer in the summer is relatively high mainly due to the expanded boundary layer. The calculation of effective ALH is introduced in Text S2. As a measure of the aerosol vertical expansion, the geometric thickness of the aerosol layer in this study is defined as the ratio of the integrated total NRB over all different levels to the maximum NRB. It is physically correlated with effective ALH driven by the expansion and collapse of the PBL. As shown in Figure 1b, these two data have a significant correlation in the boundary layer (r^2 = 0.67). This correlation can be used to construct the vertical profile together with retrieved total AOD and effective ALH in the boundary layer.

3. Retrieval of Aerosol Vertical Profile

3.1. Sensitivity Study and Spectral Sorting

To understand the impact of aerosol vertical structure on the radiance observed by CLARS, a forward RT simulation is performed using the 2S-ESS RT model (Spurr & Natraj, 2011; Zeng et al., 2017; Zhang et al., 2015). The RT model settings are described in Text S3. Figure 2a shows the aerosol layer structures in the RT model. Five aerosol layers are constructed by equally dividing the height from the surface (292 m for West Pasadena surface target) to the CLARS elevation (1,673 m). The layers are centered at 430, 706,

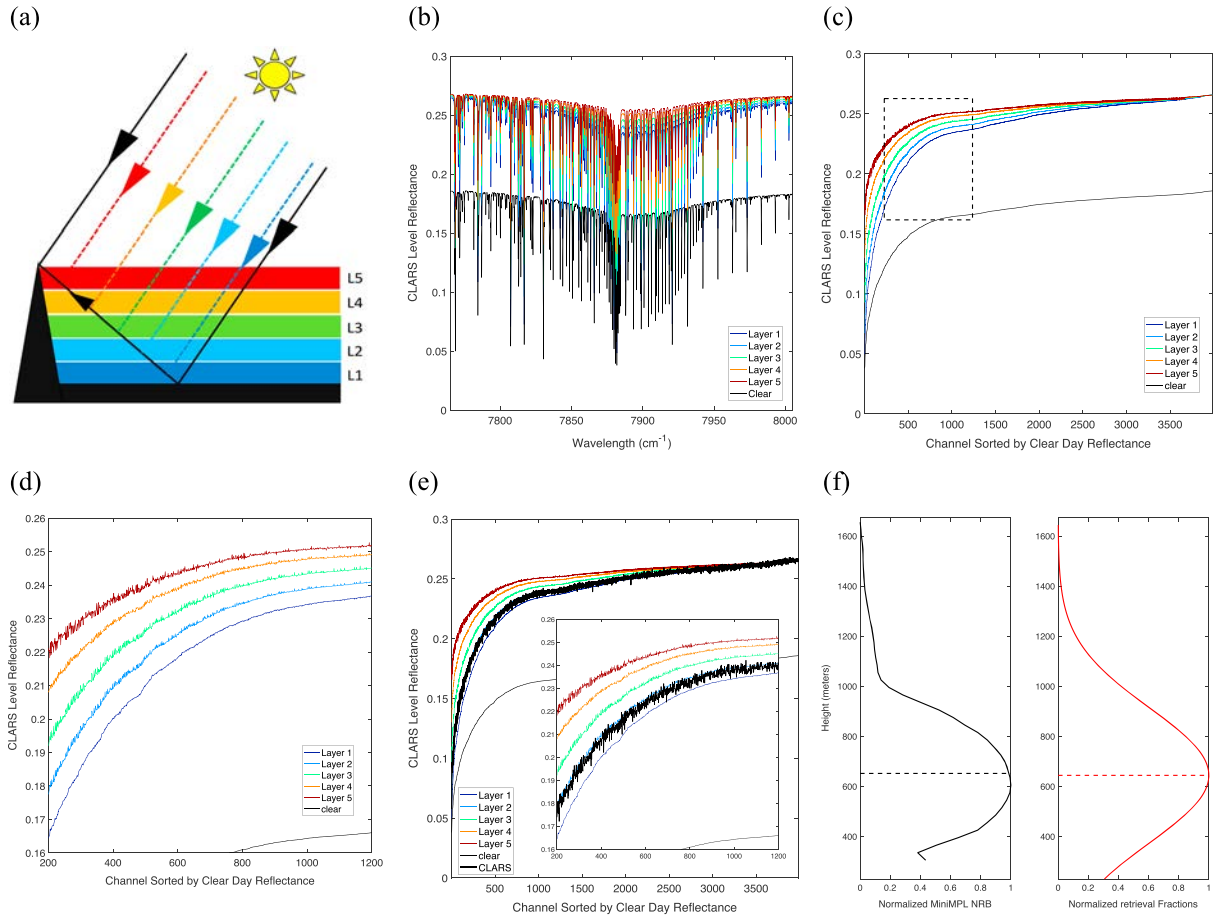

Figure 2. (a) Aerosol layer structures formulated in the radiative transfer model. Five aerosol layers are constructed by equally dividing the height from the surface (292 m above sea level for West Pasadena surface target) to the CLARS elevation (1,673 m). The layers are centered at 430, 706, 983, 1,259, and 1,535 m, respectively, with layer vertical thickness of 276 m. (b) Five aerosol layer scenarios simulated by adding the same amount of aerosol loading but in different layers. The simulated CLARS reflectance in the oxygen band is shown for the five scenarios (in blue to red from layer 1 to layer 5, respectively), as well as the clean scenario (in black). These simulations use the solar geometries at 14:00 on 17 September 2013, and collocated aerosol optical properties (single scattering albedo and phase function) from Aerosol Robotic Network. The solar zenith angle is 46.56°, and the aerosol scattering angle is 50.64°. (c) The simulated spectra from (b) sorted according to the reflectance value. The sorting order is obtained from the clear scenario spectra and then applied to all other scenarios. (d) Zoomed in plot of the rectangle shown in (c). (e) Same as (c) but overlaid with measured reflectance from CLARS. (f) Observed aerosol layer profile from MiniMPL and ALH (652 m) in the left panel, and the retrieved profile and ALH (644 m) in the right panel. The measured AOD (0.0257) and retrieved AOD (0.0279) at 1.27 μm are also indicated. The corresponding AOD at 0.5 μm is about 0.10. The MiniMPL measurements are not available below 275 m above sea level, which is the height of the building where the instrument is located. CLARS = California Laboratory for Atmospheric Remote Sensing; NRB = normalized relative backscatter; ALH = aerosol layer height; AOD = aerosol optical depth; MiniMLP = Mini MicroPulse Lidar.

983, 1,259, and 1,535 m, respectively, with a layer vertical thickness of 276 m. The selection of five layers is limited by measurement uncertainty from CLARS to build up a lookup table for ALH retrievals as described in section 3.2. Five scenarios are simulated by adding the same amount of aerosol loading but in different layers. Figure 2b shows the simulated CLARS reflectance in the 1.27-μm band for the five scenarios as well as the clear-sky scenario. Since the aerosol has a higher reflectivity than the surface, the observed radiances are significantly larger for the five aerosol cases than the clear-sky case. These simulations use the solar geometries at 14:00 LT in September 2013 and colocated aerosol optical properties (SSA and phase function) from AERONET. We can see that, for the different scenarios, the radiance values are similar in the continuum but different within the absorption bands, with stronger absorption when the aerosol layer is placed at a lower altitude. These differences are even more obvious when we sort the radiance, as shown in Figure 2c. This is done by sorting the reflectance from the clear-sky spectrum and then applying the same order to other scenarios with aerosol scattering. Using this approach, strong, medium, and weak lines appear on the left, middle, and right sections of each curve, respectively. There

are at least two pieces of information directly available from the spectral comparison: (1) the continuum level constrains the total AOD since O_2 absorption is weak and therefore the radiance is directly related to aerosol loading along the light path given surface albedo is unchanged and (2) the reflected radiance in the intermediate absorption lines, as shown in Figures 2c and 2d, exhibits large differences among the different aerosol scenarios and therefore its variability constrains ALH. The strongest absorption lines are not used in order to avoid the associated large uncertainty in the measurement (due to saturation effects). The small wiggles in the sorted radiance are caused by the fact that wavelength dependence of the oxygen absorption coefficients is different at different altitudes, which in turn is because they vary differently with pressure and temperature. The physical basis of using oxygen to study aerosol scattering is that atmospheric aerosols scatter photons back to space and therefore reduce the chance of the photons being absorbed by the oxygen, which is almost uniformly distributed in the atmosphere. Photons scattered by higher aerosol layers undergo shorter absorption paths, thereby reducing the O_2 absorption depths.

From this sensitivity study, we can see that the observed hyperspectral radiance in the oxygen band has strong sensitivities to both aerosol loading and aerosol vertical structure within the boundary layer. The spectral sorting technique provides a straightforward way to extract the information on aerosol loading and its vertical structure from the observed radiance.

3.2. AOD and ALH Retrievals

The retrieval is implemented in two steps. First, the total AOD is retrieved by constructing a lookup table with different aerosol loadings, as shown in Figures S5a and S5b, for the purpose of fitting the observed and simulated radiances in the continuum. Subsequently, another lookup table is built by placing aerosols in different layers and comparing the simulated spectra with observations, as shown in Figure 2e. The measurements are relatively noisy compared to model simulations, probably because the model simplifies some physical processes that are otherwise hard to capture. It is evident from the measurements that the effective height of the aerosol layer lies between the first (ALH: 430 m) and second (ALH: 706 m) layers, while being closer to the latter. A quantitative comparison between measurements and simulations is needed to get the exact effective ALH. To minimize the impact of data noise on the comparison, we fit the sorted spectra to quantify the spectral shape, as described in Text S4. Different metrics can be used to quantify the difference in reflectance between model simulations and measurements. Here we use the mean value of reflectance over this intermediate absorption window calculated by averaging all CLARS level reflectance values and build the lookup table, as shown in Figure S5d. The effective ALH from CLARS measurements is then retrieved by projecting on the lookup table. The geometric thickness of the aerosol layer can be derived from the correlation plot in Figure 1b. Assuming that the aerosol vertical distribution follows a normal distribution, we can reconstruct the aerosol vertical structure, as shown in Figure 2f, based on the retrieved total AOD, effective ALH, and the derived aerosol layer geometric thickness (see Text S5 for details). It is evident that the retrieved profile reproduces the vertical structure of the measured profile very well.

3.3. Assessment of Retrieval Accuracy

The retrieval accuracy of the proposed method is evaluated by applying the retrieval method to all available measurements with coincident CLARS, AERONET, and MiniMPL measurements from May 2013 to December 2014. Cases with high or low clouds are excluded using the oxygen ratio technique (K. W. Wong et al., 2015). For total AOD retrievals, 160 cases from collocated CLARS and AERONET measurements are available for this comparison, as shown in Figure 3a. The AOD ranges from 0 to 0.12 (Figure S3). Aerosol optical properties from AERONET are used in the RT model for the retrieval. The retrievals are significantly correlated with the AOD from AERONET (r^2 = 0.74; root-mean-square error, RMSE = 0.013). The total AOD retrieval has an error of 24.9% on average compared with AERONET data. Part of the variability may be due to the fact that the light paths for AERONET and CLARS are not the same. To compare the retrieved effective ALH with MiniMPL observations, data filtering is performed to ensure the validity of the measurements from AERONET and MiniMPL. First, cases with bad AOD retrieval (Figure 3a), that is, retrieval error larger than 50% (about 10% of data involved), are not used. Second, we correlate the AERONET AOD with MiniMPL backscatter data, as shown in Figure S4. Data with difference (between AERONET and MiniMPL observations) larger than 1.5 standard deviations from the mean, as indicated by red, are not included.

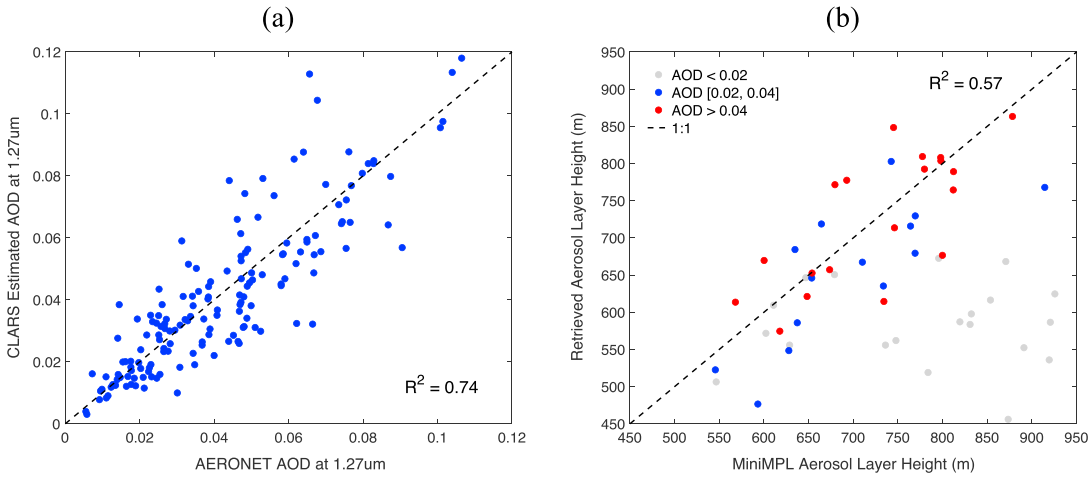

Figure 3. (a) Retrievals of total AOD at 14:00 from CLARS compared with corresponding AERONET-Caltech measurements. In total, 160 cases from collocated CLARS and AERONET measurements are available for this comparison. The retrievals are significantly correlated with the truth (r^2 = 0.74; RMSE = 0.013); (b) Retrievals of effective ALH from CLARS at 14:00 compared with the corresponding aerosol layer height derived from MiniMPL at Caltech. In total, 53 cases are available from collocated CLARS, AERONET, and MiniMPL measurements. Three different levels of aerosol loading are plotted according to AOD; retrievals for AOD larger than 0.02 are significantly correlated with the truth (r^2 = 0.57; RMSE = 67.01 m).
CLARS = California Laboratory for Atmospheric Remote Sensing; AOD = aerosol optical depth; AERONET = Aerosol Robotic Network; RMSE = root-mean-square error; MiniMLP = Mini MicroPulse Lidar.

In general, these excluded cases are those days with large aerosol heterogeneity, such that the AERONET and MiniMPL data may not be representative of aerosol conditions within the CLARS light path. In total, 53 cases are available from collocated CLARS, AERONET, and MiniMPL measurements. Three different levels of aerosol loading are plotted according to AOD. We found that retrievals for AOD larger than 0.02 are significantly correlated with the truth (r^2 = 0.57; RMSE = 67.01 m), as shown in Figure 3b. A much better performance can be found for cases with larger AOD because it provides higher aerosol scattering

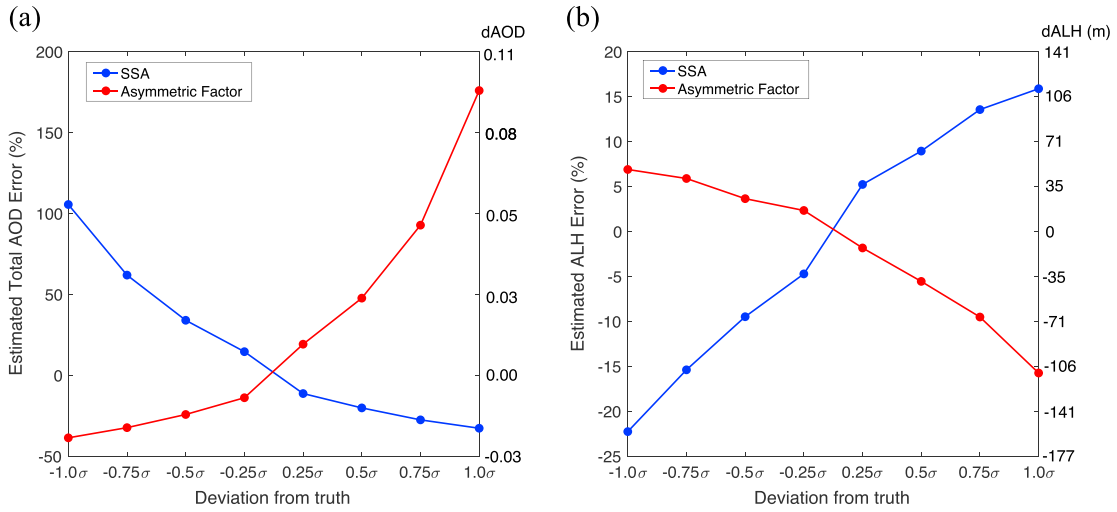

Figure 4. Uncertainty in total AOD and effective ALH retrievals from CLARS measurements caused by errors in input aerosol optical properties. The synthetic radiance observation is first generated using the same CLARS and solar geometries as in Figure 2, with aerosol in the middle layer (ALH = 706 m), and averaged total AOD (0.054), SSA (0.859), and asymmetry parameter (0.812) derived from long term Aerosol Robotic Network measurements at Caltech. The corresponding standard deviations (σ) for SSA (0.146) and asymmetry parameter (0.0877) are used as the estimation errors. The total AOD in (a) and ALH in (b) are then retrieved by applying the proposed method to the synthetic spectral data SSA or asymmetry parameter perturbed by a certain error (-1.0σ, -0.75σ, -0.5σ, -0.25σ, 0.25σ, 0.5σ, 0.75σ, 1.0σ). The estimation errors in total AOD and asymmetry parameter are calculated as the deviation (in percentage) from the known truth. SSA = single scattering albedo; AOD = aerosol optical depth; ALH = aerosol layer height; CLARS = California Laboratory for Atmospheric Remote Sensing.

signal that can be captured by CLARS. When aerosol loading is weak, the aerosol scattering signal may be negligible compared to that from surface reflectance. Therefore, the retrieved effective ALH tends to be smaller than the truth and closer to the surface. The AOD of 0.02 at 1.27 μm corresponds to about 0.085 at 0.50 μm based on the averaged Ångström coefficients that are related to the aerosol composition. The effective ALH retrieval has an error of 7.8% on average compared with the corresponding MiniMPL data. Overall, the proposed algorithm can accurately capture the variability of the total AOD and effective ALH in the PBL.

3.4. Impacts of SSA and Phase Function

The proposed profiling technique uses inversion products of SSA and phase function from AERONET in the study area and assumes that we have accurate estimates of these products, which may not always be the case. Here we quantify the retrieval uncertainty on total AOD and effective ALH caused by errors in the SSA and phase function. For simplicity, the aerosol scattering in the model is assumed to follow the Henyey-Greenstein type phase function (Henyey & Greenstein, 1941), which depends solely on the asymmetry parameter. The results are shown in Figure 4. As the SSA increases, the aerosols appear brighter; therefore, the estimated total AOD is lower to match the observed radiance. On the other hand, the estimated ALH increases because, for a given aerosol loading, a greater degree of scattering arises due to a shorter light path, as seen in the sensitivity study in Figure 2b. The effects of asymmetry parameter have a different pattern. As the asymmetry parameter increases, the phase function has a stronger peak in the forward direction (scattering angle less than 20°) and a smaller fraction in the remaining scattering angles including the angle (50.64°) used in this simulation. In general, the error in total AOD retrieval is higher than that in ALH retrieval. As indicated by Figure 3, the RMSE in total AOD (0.013) is about 25% of the averaged total AOD (0.0541) in this simulation, while the RMSE in effective ALH (67 m) is about 10% of the true ALH (706 m). These error fractions are approximately comparable to the estimated errors due to a deviation of $\pm 0.5\sigma$ in SSA and asymmetry parameter (Figure 4). A discussion on obtaining SSA and phase function from satellite retrievals and model simulations is provided in Text S6.

4. Conclusions

This work represents the first attempt to profile boundary layer aerosol vertical structure using hyperspectral remote sensing measurements. The proposed algorithm, which uses hyperspectral measurements in the 1.27-μm oxygen absorption band to retrieve the total AOD and the effective ALH, is applied to data from the CLARS-FTS instrument, located on a mountaintop overlooking the LA basin. The effectiveness and accuracy of the retrievals are assessed by comparing with AOD from AERONET and backscatter profile from MiniMPL lidar measurements. The spectral sorting technique provides two advantages over a conventional fitting scheme: (1) information related to aerosol loading and its vertical structure can be extracted in a straightforward manner from the observed radiance and (2) the spectral region(s) with the largest sensitivity to arbitrary geophysical retrieval parameters (total AOD and ALH in this study) can be identified. The proposed retrieval algorithm to constrain aerosol vertical distribution will potentially help quantify the aerosol direct radiative forcing and reduce bias in greenhouse gas retrievals from space due to uncertainty caused by aerosol scattering.

The algorithm developed in this study has two implications for analyzing spaceborne observations, such as hyperspectral O_2 A-band measurements from the OCO-2 (Crisp et al., 2012) and the upcoming OCO-3 (Eldering et al., 2013) missions. First, accuracy of ALH retrieval shows a certain dependence on SSA and phase function, whose retrieval accuracies can be further improved by combining hyperspectral oxygen absorption and polarimetric measurements in a broad spectral range (e.g., ultraviolet-near infrared of Airborne Multiangle SpectroPolarimetric Imager [Diner et al., 2005; F. Xu, van Harten, et al., 2017; X. Xu, Wang, et al., 2017] and ultraviolet-shortwave infrared of Research Scanning Polarimeter [Cairns et al., 1999; Wu et al., 2015]) to simultaneously determine aerosol profile and microphysical properties as well as surface reflection. Moreover, polarization measurements may also improve the aerosol layer detection over bright surfaces (see the discussion on surface albedo in Text S7). Second, a larger viewing angle off-nadir measurement provides more aerosol information, for example, OCO-3 off-nadir measurements with the urban target mode. In the near future, CLARS-FTS will be upgraded to include measurements in the O_2 A-band at 0.76 μm. The O_2 A-band is more sensitive to scattering from fine mode aerosols while the O_2 $^1\Delta$ band at 1.27 μm is more

sensitive to scattering from coarse mode aerosols. A combination of these spectral regions may help to distinguish the profiles of fine and coarse mode aerosols.

Acknowledgments
We thank Jack Margolis, Chao Liu, Yuan Wang, Siteng Fan, Suniti Sanghavi, Mike Gunson, and Annmarie Eldering for stimulating discussions. V. N. acknowledges support from the NASA Earth Science US Participating Investigator program (solicitation NNH16ZDA001N-ESUSPI). F. X. acknowledges support from NASA Remote Sensing Theory program under grant 14-RST14-0100. We are also thankful for the support from the Jet Propulsion Laboratory Research and Technology Development Program. Part of the research in this study was performed at the Jet Propulsion Laboratory, California Institute of Technology, under a contract with the National Aeronautics and Space Administration. The CLARS project receives support from the California Air Resources Board and the NIST GHG and Climate Science Program. The MiniMPL was supported by the KISS Program at Caltech; data are available from the NASA Megacity project data portal: https://megacities.jpl.nasa.gov/portal/. AERONET data for the Caltech site are available from https://aeronet.gsfc.nasa.gov/new_web/photo_db_v3/CalTech.html. We also thank Jochen Stutz from UCLA and his staff for their effort in establishing and maintaining the AERONET Caltech site. CLARS-FTS data are available from the authors upon request, and part of the data are available from the NASA Megacities Project at https://megacities.jpl.nasa.gov. We are grateful to the two anonymous reviewers whose comments helped improve the paper.

References

Butz, A., Hasekamp, O. P., Frankenberg, C., & Aben, I. (2009). Retrievals of atmospheric CO_2 from simulated space-borne measurements of backscattered near-infrared sunlight: Accounting for aerosol effects. *Applied Optics*, *48*(18), 3322–3336. https://doi.org/10.1364/AO.48.003322

Cairns, B., Russell, E. E., & Travis, L. D. (1999). Research scanning polarimeter: Calibration and ground-based measurements. In *Polarization: Measurement, analysis, and remote sensing II, Proc. SPIE* (Vol. 3754, pp. 186–197). Denver, CO: International Society for Optics and Photonics. https://doi.org/10.1117/12.366329

Colosimo, S. F., Natraj, V., Sander, S. P., & Stutz, J. (2016). A sensitivity study on the retrieval of aerosol vertical profiles using the oxygen A-band. *Atmospheric Measurement Techniques*, *9*(4), 1889–1905. https://doi.org/10.5194/amt-9-1889-2016

Crisp, D., Fisher, B. M., O'Dell, C., Frankenberg, C., Basilio, R., Bösch, H., et al. (2012). The ACOS CO_2 retrieval algorithm—Part II: Global XCO_2 data characterization. *Atmospheric Measurement Techniques*, *5*(4), 687–707. https://doi.org/10.5194/amt-5-687-2012

Davis, A. B., Kalashnikova, O. V., and Diner, D. J. (2017). Aerosol layer height over water from O_2 A-band: mono-angle hyperspectral and/or bi-spectral multi-angle observations. Preprint, https://doi.org/10.20944/preprints201710.0055.v1

Diner, D. J., Beckert, J. C., Reilly, T. H., Bruegge, C. J., Conel, J. E., & Kahn, R. A. (1998). Multi-angle Imaging SpectroRadiometer (MISR) instrument description and experiment overview. *IEEE Transactions on Geoscience and Remote Sensing*, *36*(4), 1072–1087. https://doi.org/10.1109/36.700992

Diner, D. J., Braswell, B. H., Davies, R., Gobron, N., Hu, J., Jin, Y., et al. (2005). The value of multiangle measurements for retrieving structurally and radiatively consistent properties of clouds, aerosols, and surfaces. *Remote Sensing of Environment*, *97*(4), 495–518. https://doi.org/10.1016/j.rse.2005.06.006

Ding, S., Wang, J., & Xu, X. (2016). Polarimetric remote sensing in oxygen A and B bands: Sensitivity study and information content analysis for vertical profile of aerosols. *Atmospheric Measurement Techniques*, *9*(5), 2077–2092. https://doi.org/10.5194/amt-9-2077-2016

Dubuisson, P., Frouin, R., Dessailly, D., Duforêt, L., Léon, J.-F., Voss, K., & Antoine, D. (2009). Estimating the altitude of aerosol plumes over the ocean from reflectance ratio measurements in the O_2 A-band. *Remote Sensing of Environment*, *113*(9), 1899–1911. https://doi.org/10.1016/j.rse.2009.04.018

Eldering, A., Kaki, S., Crisp, D., & Gunson, M. R. (2013). The OCO-3 mission. Abstracts A21G-0134 presented at 2013 Fall Meeting, American Geophysical Union, San Francisco, CA, 9–13 Dec.

Frankenberg, C., Butz, A., & Toon, G. C. (2011). Disentangling chlorophyll fluorescence from atmospheric scattering effects in O_2 A-band spectra of reflected sun-light. *Geophysical Research Letters*, *38*, L03801. https://doi.org/10.1029/2010GL045896

Fu, D., Pongetti, T. J., Blavier, J.-F. L., Crawford, T. J., Manatt, K. S., Toon, G. C., et al. (2014). Near-infrared remote sensing of Los Angeles trace gas distributions from a mountaintop site. *Atmospheric Measurement Techniques*, *7*(3), 713–729. https://doi.org/10.5194/amt-7-713-2014

Gabella, M., Kisselev, V., & Perona, G. (1999). Retrieval of aerosol profile variations from reflected radiation in the oxygen absorption a band. *Applied Optics*, *38*(15), 3190–3195. https://doi.org/10.1364/AO.38.003190

Geddes, A., & Bösch, H. (2015). Tropospheric aerosol profile information from high-resolution oxygen A-band measurements from space. *Atmospheric Measurement Techniques*, *8*(2), 859–874. https://doi.org/10.5194/amt-8-859-2015

Heidinger, A., & Stephens, G. L. (2000). Molecular line absorption in a scattering atmosphere, Part II: Application to remote sensing in the O_2 A-band. *Journal of the Atmospheric Sciences*, *57*(10), 1615–1634. https://doi.org/10.1175/1520-0469

Henyey, L. G., & Greenstein, J. L. (1941). Diffuse radiation in the galaxy. *The Astrophysical Journal*, *93*, 70–83.

Holben, B. N., Eck, T. F., Slutsker, I., Tanre, D., Buis, J. P., & Setzer, A. (1998). AERONET—A federated instrument network and data archive for aerosol characterization. *Remote Sensing of Environment*, *66*(1–16), 1998.

Hollstein, A., & Fischer, J. (2014). Retrieving aerosol height from the oxygen A band: A fast forward operator and sensitivity study concerning spectral resolution, instrumental noise, and surface inhomogeneity. *Atmospheric Measurement Techniques*, *7*(5), 1429–1441. https://doi.org/10.5194/amt-7-1429-2014

Hou, W., Wang, J., Xu, X., & Reid, J. S. (2017). An algorithm for hyperspectral remote sensing of aerosols: 2. Information content analysis for aerosol parameters and principal components of surface spectra. *Journal of Quantitative Spectroscopy & Radiative Transfer*, *192*, 14–29. https://doi.org/10.1016/j.jqsrt.2017.01.041

Intergovernmental Panel on Climate Change (2013). In T. F. Stocker, et al. (Eds.), *Climate change 2013: The Physical Science Basis. Contribution of Working Group I to the Fifth Assessment Report of the Intergovernmental Panel on Climate Change* (pp. 595–605). Cambridge, UK, and New York: Cambridge University Press. https://doi.org/10.1017/CBO9781107415324

Irion, F. W., Gunson, M. R., Toon, G. C., Chang, A. Y., Eldering, A., Mahieu, E., et al. (2002). Atmospheric Trace Molecule Spectroscopy (ATMOS) experiment version 3 data retrievals. *Applied Optics*, *41*(33), 6968–6979. https://doi.org/10.1364/AO.41.006968

Jethva, H., Torres, O., & Ahn, C. (2014). Global assessment of OMI aerosol single-scattering albedo using ground-based AERONET inversion. *Journal of Geophysical Research: Atmospheres*, *119*, 9020–9040. https://doi.org/10.1002/2014JD021672

Kahn, R. A., Garay, M. J., Nelson, D. L., Yau, K. K., Bull, M. A., Gaitley, B. J., et al. (2007). Satellite-derived aerosol optical depth over dark water from MISR and MODIS: Comparisons with AERONET and implications for climatological studies. *Journal of Geophysical Research*, *112*, D18205. https://doi.org/10.1029/2006JD008175

Kalnay, E., Kanamitsu, M., Kistler, R., Collins, W., Deaven, D., Gandin, L., et al. (1996). The NCEP/NCAR 40-year reanalysis project. *Bulletin of the American Meteorological Society*, *77*(3), 437–471. https://doi.org/10.1175/1520-0477(1996)077<0437:TNYRP>2.0.CO;2

Kinne, S., Lohmann, U., Feichter, J., Schulz, M., Timmreck, C., Ghan, S., et al. (2003). Monthly averages of aerosol properties: A global comparison among models, satellite data, and AERONET ground data. *Journal of Geophysical Research*, *108*(D20), 4634. https://doi.org/10.1029/2001JD001253

Koffi, B., Schulz, M., Bréon, F. M., Griesfeller, J., Winker, D., Balkanski, Y., et al. (2012). Application of the CALIOP layer product to evaluate the vertical distribution of aerosols estimated by global models: AeroCom phase I results. *Journal of Geophysical Research*, *117*, D10201. https://doi.org/10.1029/2011JD016858

Kuang, Z. M., Margolis, J., Toon, G., Crisp, D., & Yung, Y. L. (2002). Spaceborne measurements of atmospheric CO_2 by high-resolution NIR spectrometry of reflected sunlight: An introductory study. *Geophysical Research Letters*, *29*(15), 1716. https://doi.org/10.1029/2001GL014298

Liu, Y., & Diner, D. J. (2017). Multi-angle imager for aerosols: A satellite investigation to benefit public health. *Public Health Reports*, *132*(1), 14–17. https://doi.org/10.1177/0033354916679983

O'Brien, D. M., & Mitchell, R. M. (1992). Error estimates for retrieval of cloud-top pressure using absorption in the A-band of oxygen. *Journal of Applied Meteorology*, *31*(10), 1179–1192. https://doi.org/10.1175/1520-0450(1992)031<1179:EEFROC>2.0.CO;2

O'Dell, C. W., Connor, B., Bösch, H., O'Brien, D., Frankenberg, C., Castano, R., et al. (2012). The ACOS CO_2 retrieval algorithm—Part 1: Description and validation against synthetic observations. *Atmospheric Measurement Techniques*, *5*, 99–121. https://doi.org/10.5194/amt-5-99-2012

Richardson, M., McDuffie, J., Stephens, G. L., Cronk, H. Q., & Taylor, T. E. (2017). The OCO-2 oxygen A-band response to liquid marine cloud properties from CALIPSO and MODIS. *Journal of Geophysical Research: Atmospheres*, *122*, 8255–8275. https://doi.org/10.1002/2017JD026561

Sanghavi, S., Martonchik, J. V., Landgraf, J., & Platt, U. (2012). Retrieval of aerosol optical depth and vertical distribution using O_2 A- and B-band SCIAMACHY observations over Kanpur: A case study. *Atmospheric Measurement Techniques*, *5*(5), 1099–1119. https://doi.org/10.5194/amt-5-1099-2012

Seinfeld, J., & Pandis, S. (2006). *Atmospheric chemistry and physics: From air pollution to climate change* (p. 1224). New Jersey: John Wiley.

Sen, B., Toon, G. C., Blavier, J.-F., Fleming, E. L., & Jackman, C. H. (1996). Balloon-borne observations of mid-latitude fluorine abundance. *Journal of Geophysical Research*, *101*(D4), 9045–9054. https://doi.org/10.1029/96JD00227

Spurr, R. J. D., & Natraj, V. (2011). A linearized 2-stream radiative transfer code for fast approximation of multiple-scatter fields. *Journal of Quantitative Spectroscopy & Radiative Transfer*, *112*(16), 2630–2637. https://doi.org/10.1016/j.jqsrt.2011.06.014

Timofeyev, Y. M., Vasilyev, A. V., & Rozanov, V. V. (1995). Information content of the spectral measurements of the 0.76 μm O_2 outgoing radiation with respect to the vertical aerosol optical properties. *Advances in Space Research*, *16*(10), 91–94. https://doi.org/10.1016/0273-1177(95)00385-R

Torres, O., Bhartia, P. K., Herman, J. R., Ahmad, Z., & Gleason, J. (1998). Derivation of aerosol properties from satellite measurements of backscattered ultraviolet radiation: Theoretical basis. *Journal of Geophysical Research*, *103*(D14), 17,099–17,110.

Wang, J., Xu, X., Ding, S., Zeng, J., Spurr, R., Liu, X., et al. (2014). A numerical testbed for remote sensing of aerosols, and its demonstration for evaluating retrieval synergy from a geostationary satellite constellation of GEO-CAPE and GOES-R. *Journal of Quantitative Spectroscopy & Radiative Transfer*, *146*, 510–528. https://doi.org/10.1016/j.jqsrt.2014.03.020

Ware, J., Kort, E. A., DeCola, P., & Duren, R. (2016). Aerosol lidar observations of atmospheric mixing in Los Angeles: Climatology and implications for greenhouse gas observations. *Journal of Geophysical Research: Atmospheres*, *121*, 9862–9878. https://doi.org/10.1002/2016JD024953

Winker, D. M., Vaughan, M. A., Omar, A., Hu, Y., Powell, K. A., Liu, Z., et al. (2009). Overview of the CALIPSO mission and CALIOP data processing algorithms. *Journal of Atmospheric and Oceanic Technology*, *26*(11), 2310–2323. https://doi.org/10.1175/2009JTECHA1281.1

Wong, C. K., Pongetti, T. J., Oda, T., Rao, P., Gurney, K. R., Newman, S., et al. (2016). Monthly trends of methane emissions in Los Angeles from 2011 to 2015 inferred by CLARS-FTS observations. *Atmospheric Chemistry and Physics*, *16*(20), 13,121–13,130. https://doi.org/10.5194/acp-16-13121-2016

Wong, K. W., Fu, D., Pongetti, T. J., Newman, S., Kort, E. A., Duren, R., et al. (2015). Mapping CH4: CO_2 ratios in Los Angeles with CLARS-FTS from Mount Wilson, California. *Atmospheric Chemistry and Physics*, *15*, 241–2252. https://doi.org/10.5194/acp-15-241-2015

Wu, L., Hasekamp, O., van Diedenhoven, B., & Cairns, B. (2015). Aerosol retrieval from multiangle, multispectral photopolarimetric measurements: Importance of spectral range and angular resolution. *Atmospheric Measurement Techniques*, *8*(6), 2625–2638. https://doi.org/10.5194/amt-8-2625-2015

Wunch, D., Toon, G. C., Blavier, J.-F. L., Washenfelder, R. A., Notholt, J., Connor, B. J., et al. (2011). The total carbon column observing network. *Philosophical Transactions of the Royal Society A: Mathematical, Physical and Engineering Sciences*, *369*(1943), 2087–2112. https://doi.org/10.1098/rsta.2010.0240

Xi, X., Natraj, V., Shia, R. L., Luo, M., Zhang, Q., Newman, S., et al. (2015). Simulated retrievals for the remote sensing of CO_2, CH_4, CO, and H_2O from geostationary orbit. *Atmospheric Measurement Techniques*, *8*(11), 4817–4830. https://doi.org/10.5194/amt-8-4817-2015

Xu, F., van Harten, G., Diner, D. J., Kalashnikova, O. V., Seidel, F. C., Bruegge, C. J., & et al. (2017). Coupled retrieval of aerosol properties and land surface reflection using the Airborne Multiangle SpectroPolarimetric Imager (AirMSPI). *Journal of Geophysical Research: Atmospheres*, *122*, 7004–7026.

Xu, X., Wang, J., Wang, Y., Zeng, J., Torres, O., Yang, Y., et al. (2017). Passive remote sensing of altitude and optical depth of dust plumes using the oxygen A and B bands: First results from EPIC/DSCOVR at Lagrange-1 point. *Geophysical Research Letters*, *44*, 7544–7554. https://doi.org/10.1002/2017GL073939

Yamamoto, G., & Wark, D. Q. (1961). Discussion of the letter by R.A. Hanel, Determination of cloud altitude from a satellite. *Journal of Geophysical Research*, *66*(10), 3596. https://doi.org/10.1029/JZ066i010p03596

Zarzycki, C. M., & Bond, T. C. (2010). How much can the vertical distribution of black carbon affect its global direct radiative forcing? *Geophysical Research Letters*, *37*, L20807. https://doi.org/10.1029/2010GL044555

Zeng, Z.-C., Zhang, Q., Natraj, V., Margolis, J. S., Shia, R.-L., Newman, S., et al. (2017). Aerosol scattering effects on water vapor retrievals over the Los Angeles Basin. *Atmospheric Chemistry and Physics*, *17*(4), 2495–2508. https://doi.org/10.5194/acp-17-2495-2017

Zhang, Q., Natraj, V., Li, K.-F., Shia, R.-L., Fu, D., Pongetti, T. J., et al. (2015). Accounting for aerosol scattering in the CLARS retrieval of column averaged CO_2 mixing ratios. *Journal of Geophysical Research: Atmospheres*, *120*, 7205–7218. https://doi.org/10.1002/2015JD023499

Zhang, Q., Shia, R.-L., Sander, S. P., & Yung, Y. L. (2016). XCO_2 retrieval error over deserts near critical surface albedo. *Earth and Space Science*, *3*, 36–45. https://doi.org/10.1002/2015EA000143

Supporting information for:

Constraining aerosol vertical profile in the boundary layer using hyperspectral measurements of oxygen absorption

Zhao-Cheng Zeng[1], Vijay Natraj[2], Feng Xu[2], Thomas J. Pongetti[2], Run-Lie Shia[1], Eric A. Kort[3], Geoffrey C. Toon[2], Stanley P. Sander[2], and Yuk L. Yung[1,2]

[1] Division of Geological and Planetary Sciences, California Institute of Technology

[2] Jet Propulsion Laboratory, California Institute of Technology

[3] Department of Climate and Space Sciences and Engineering, University of Michigan

Correspondence to zcz@gps.caltech.edu

Contents:

Text S1: AOD extrapolation using Ångström exponent law

The AERONET site at Caltech makes measurements of total AOD, from which aerosol optical properties including single scattering albedo (SSA) and phase function can be retrieved. The wavelength range covered by AERONET-Caltech measurements ranges from 340 to 1020 nm. The AOD value in the O_2 $^1\Delta$ band at 1.27 μm can be estimated using the Ångström exponent law (Seinfeld and Pandis, 2006; Zhang et al., 2015):

$$\frac{\tau}{\tau_0} = \left(\frac{\lambda}{\lambda_0}\right)^{-k} \quad (1)$$

where λ and τ are the wavelength and the corresponding AOD to be interpolated, respectively; λ_0 and τ_0 are the reference wavelength and the corresponding AOD from AERONET, respectively; and k is the Ångström exponent. The k value is obtained by applying linear regression (using the logarithmic form of Equation (1)) to the AERONET AOD measurements at six different wavelengths (340, 380, 440, 500, 870, and 1020 nm).

Text S2: Calculation of aerosol layer height (ALH)

The ALH, which is the center of mass of the scatterers, is calculated in a similar way to Xu et al. (2017) and Koffi et al. (2012):

$$ALH_{MiniMPL} = \frac{\sum_{i=1}^{n} \beta_i \cdot Z_i}{\sum_{i=1}^{n} \beta_i} \quad (2)$$

β_i and Z_i are, respectively, the backscatter signal and the height at level i.

Text S3: GFIT and 2S-ESS models

Gas absorption coefficients and ray paths are computed using the GFIT model (Sen et al., 1996). GFIT has been used extensively for quantitative analysis of solar absorption spectra of the Earth's atmosphere, including the ATMOS shuttle spectra (Irion et al., 2002) and ground based TCCON spectra (Wunch et al., 2011). Surface pressure and atmospheric pressure profiles, which are associated with oxygen vertical distribution, are obtained from the NCEP–NCAR reanalysis

dataset (Kalnay et al., 1996) on a daily basis. Details of the atmospheric profiles of trace gas volume mixing ratio, pressure and temperature used in GFIT are described in Fu et al. (2014).

The 2S-ESS model performs an exact computation of the single scattering using all moments of the phase function, while the multiply scattered radiation is calculated using the two-stream approximation. This model has been used for greenhouse gas (GHG) remote sensing in several previous studies (Xi et al., 2015; Zhang et al., 2015, 2016; Zeng et al., 2017). Aerosol optical properties, including SSA and phase function, are taken from AERONET measurements at Caltech, as mentioned in Section 2.2. The total AOD value used in the model is optimized to match the CLARS radiance measurement, as described in Section 3.2.

Text S4: Fitting of sorted spectra

To minimize the impact of data noise on the comparison, we fit the sorted spectra using Equation (3), which is formulated to quantify the spectral shape:

$$f(x) = a_1 - a_2 * (1 - x) - a_3 * \exp(-a_4 * x) \quad (3)$$

where a_1 is the largest radiance at the continuum level; a_2, a_3, and a_4 are parameters to be fitted. x is the sorted channel number, ranging from 1 to 3982, and normalized to be between 0 and 1 when doing the fitting. Assuming the absorption lines are well resolved, then the exponential part of the formula, based on the Beer-Lambert extinction law, approximates the oxygen line by line and collision-induced absorptions. The linear part of the formula is used to provide a first order approximation of the continuum shape (e.g. continuum tilt) and the variation of the instrument response across the window that are not accounted by the exponential part. Even when the spectral absorption lines are not fully resolved, we found this formula well capture the spectral shape. The spectral data are filtered by excluding anomalous data more than 1.5 standard deviations away from the mean and the nonlinear fit is then implemented using a standard least squares regression. The fitting results are shown in Figure S5(c).

Text S5: Retrieval using look-up tables (LUTs)

As shown in Figure S5, two LUTs are built to successively retrieve the total AOD and effective ALH. The total AOD is retrieved using the observed CLARS-level reflectance at the continuum

level (Figure S5(b)). On the other hand, the reflectance in the intermediate absorption window is used to retrieve the effective ALH (Figure S5(d)). Using the retrieved effective ALH, the geometric thickness (GT) of the aerosol layer can be derived from the empirical correlation as shown in Figure 1(b). As described in Section 2.3, the GT of the aerosol layer in this study is defined as the ratio of the integrated total aerosol loading (represented by NRB) over all different levels to the maximum aerosol loading.

The retrieved profile in Figure 2(f) is reconstructed by assuming a Gaussian distribution. The mean (μ) of this distribution is the retrieved effective ALH, while the standard deviation (σ) is calculated in the following way. An aerosol vertical profile following the Gaussian distribution is given by:

$$f(x) = \frac{1}{\sigma\sqrt{2\pi}} \exp\left(\frac{-(x-\mu)^2}{2\sigma^2}\right) \quad (3)$$

where x is the height and $f(x)$ is the aerosol vertical profile. The maximum value of the profile is $\frac{1}{\sigma\sqrt{2\pi}}$ when $x = \mu$. Since the integral of the Gaussian distribution $f(x)$ is unity, the GT of this profile, defined as the ratio of integrated $f(x)$ to the maximum value $\frac{1}{\sigma\sqrt{2\pi}}$, is $\sigma\sqrt{2\pi}$. As a result, $\sigma = \mathrm{GT}/\sqrt{2\pi}$. Using the retrieved μ and calculated σ, the aerosol vertical profile can be constructed as shown in Figure 2(f).

Text S6: Phase function and SSA from satellite observations and model simulations

Knowledge of the aerosol phase function and SSA are important caveats in applying the proposed algorithm. These parameters can be obtained using AERONET measurements. However, in the absence of AERONET data, satellite observations and/or model simulations can also be employed to characterize them. For example, the phase function can be retrieved using MISR (Diner et al., 2005) with its multi-angle capability, while SSA can be retrieved from several different instruments and simulations by global chemical models with improving accuracy (e.g., Jethva et al., 2014; Kinne et al., 2003). On the other hand, ALH is much less constrained (higher uncertainty in retrievals) by current measurements or model simulations. Therefore, the proposed algorithm has the potential to be applied on a global scale (including regions without AERONET measurements) to derive aerosol parameters that are currently unavailable.

Text S7: Calculation of surface albedo from CLARS-FTS measurements

One of the advantages of the CLARS geometry is that the surface albedo (shown in Figure S2(b)) can be calculated by dividing SVO-observed (incident sunlight) by LABS-observed (reflected sunlight) radiance on clear days using measurements at continuum wavelengths where gas absorption can be ignored. These derived surface albedos are used in the 2S-ESS RT model. In this study, the assumed surface albedos between 0.15 and 0.20 are typical values for urban settings such as those in Los Angeles. For bright surfaces such as deserts, the accuracy of this method needs further investigation. Conceptually, if the surface reflectance is large, then the relative contribution from aerosol to the total observed radiance is small. With smaller contribution from aerosol scattering, the look-up tables in Figures S5(a) and (c) will have smaller spectral variability for different AOD and ALH scenarios. As a result, the smaller spectral variability will lead to a larger uncertainty in retrievals. Wang et al. (2014) and Ding et al. (2016) have shown that, for bright surfaces, the sensitivity of radiance to ALH decreases. They recommend polarimetric measurements to improve sensitivity.

(a) (b)

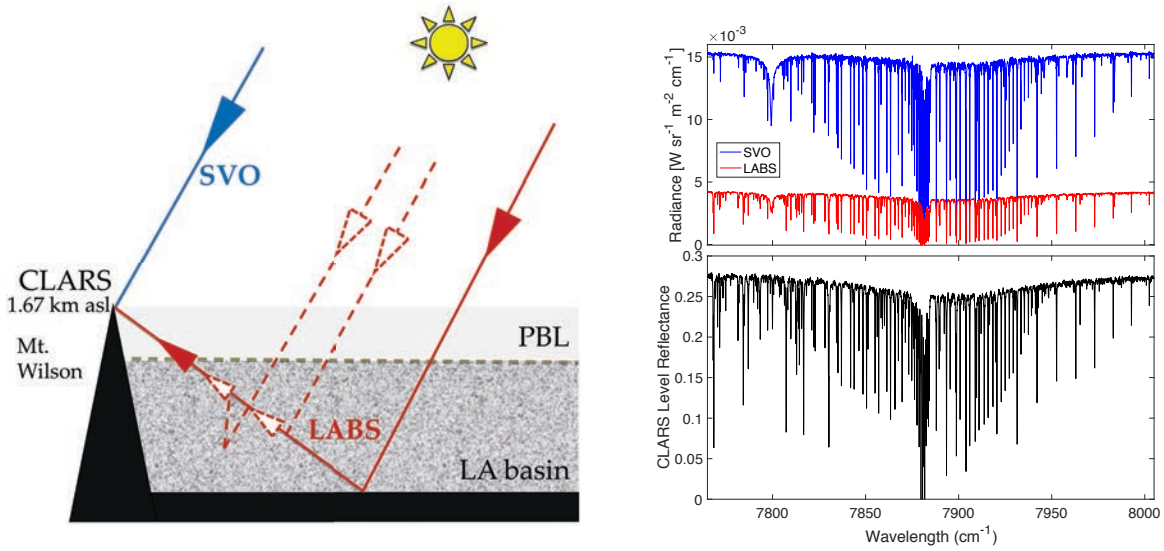

Figure S1. (a) Schematic figure of CLARS observation over the Los Angeles basin. CLARS has two modes of operation: the Los Angeles Basin Survey mode (LABS; in solid red) and the Spectralon Viewing Observation mode (SVO; in blue). An example of light path changes due to aerosol scattering along the path from the basin to the mountain top is illustrated (single and multiple scattering in dotted red); (b) Examples of CLARS-FTS measurements in the oxygen band at 1.27 μm. The top panel shows the observed radiance from SVO (blue) and LABS (red) modes, where the LABS measurements are acquired over the West Pasadena surface target. These measurements are made at 14:00 h on September 17, 2013 with a solar zenith angle of 46.43°. The bottom panel shows the CLARS level reflectance, which is the ratio of the LABS and SVO radiances shown in the top panel.

(a)

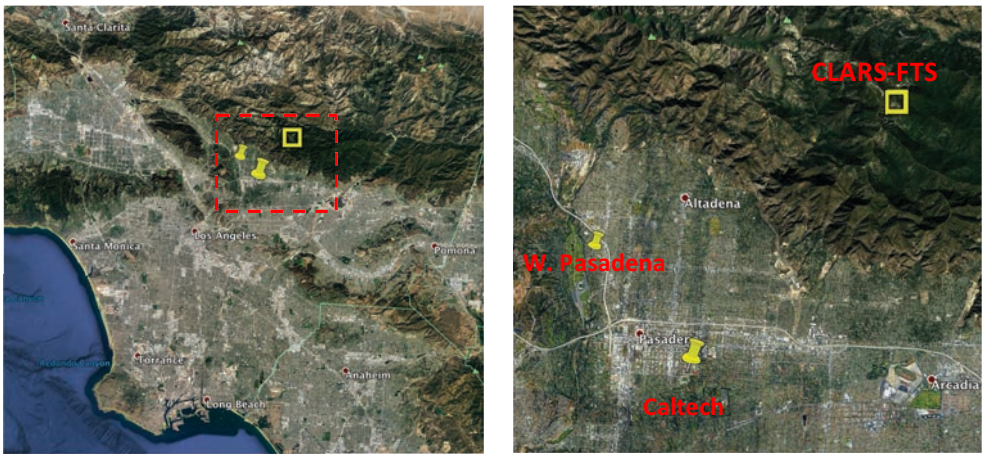

(b)

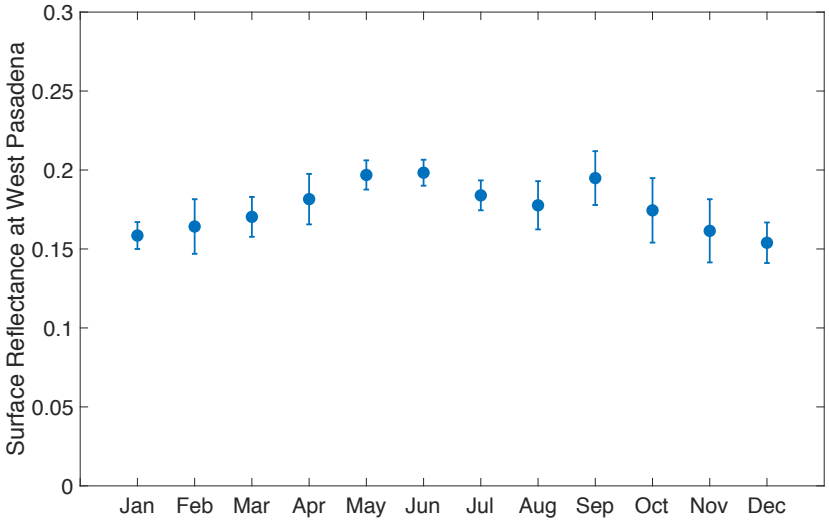

Figure S2. (a) Locations of the CLARS FTS instrument, the West Pasadena surface target, and Caltech (where the AERONET and MiniMPL instruments are located). The horizontal distance from the West Pasadena surface reflection point to Caltech is about 5 km, and that from CLARS-FTS to both West Pasadena and Caltech is about 11 km; (b) Monthly averaged surface reflectance at 1.24 μm at West Pasadena. The surface albedo at a particular surface target can be estimated by dividing SVO-observed (incident sunlight) by LABS-observed (reflected sunlight) radiance on relatively clean days using continuum wavelengths in the 1.24 μm spectral region where gas and aerosol extinction can be ignored. A scale factor is derived using the 2S-ESS RT model to correct for small effects from aerosol scattering using, the AOD and aerosol optical properties obtained from the AERONET instrument at Caltech. The error bars (one standard deviation) indicate the uncertainty in the surface albedo estimates.

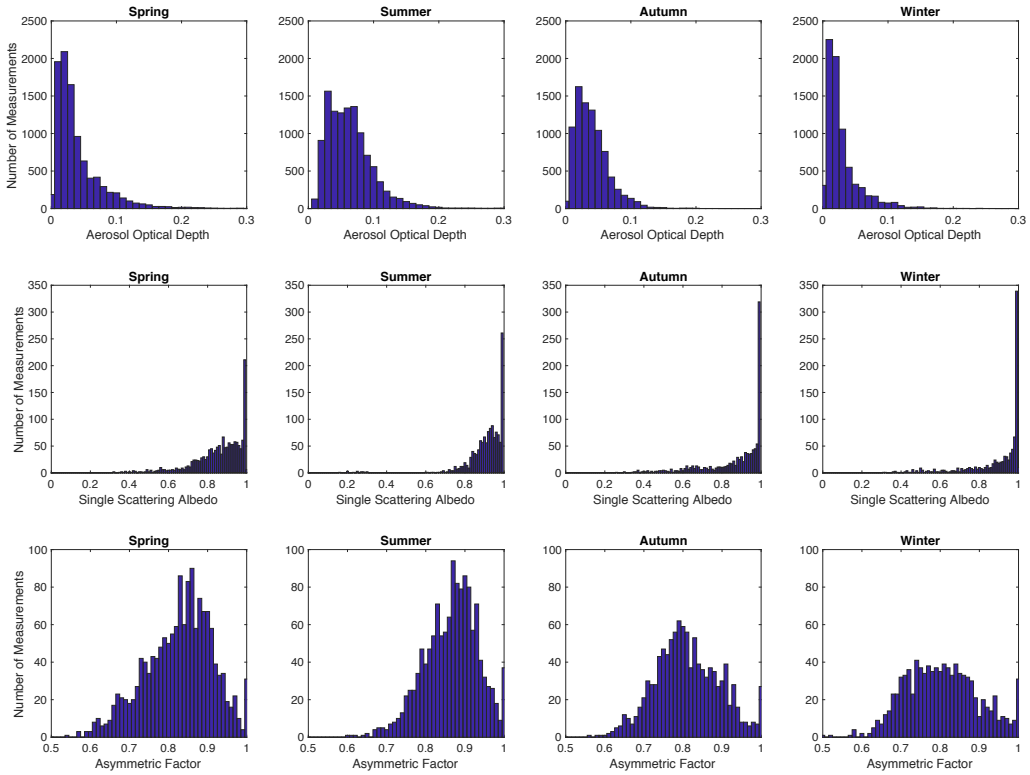

Figure S3. Monthly histograms of (top) aerosol optical depth; (middle) single scattering albedo; and (bottom) asymmetry parameter obtained from AERONET measurements at Caltech from 2011 to 2017.

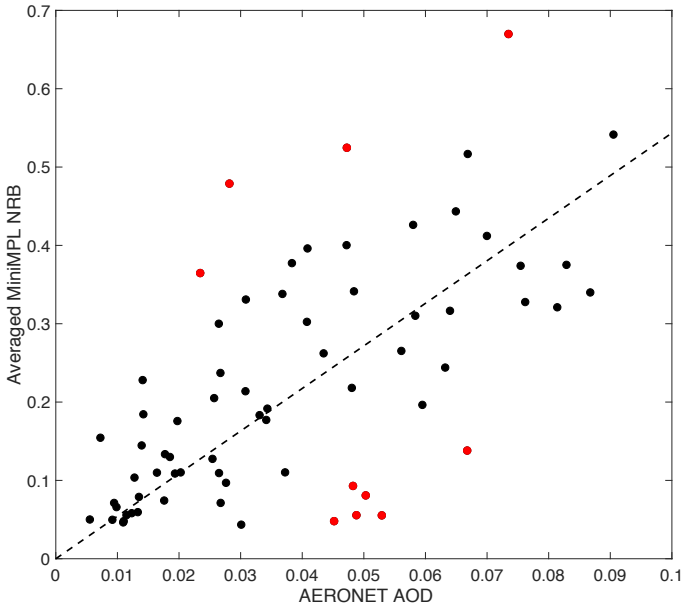

Figure S4. Correlation plot between averaged MiniMPL normalized relative backscatter signal and AERONET AOD at 1.27 μm. Measurements that deviate by more than 1.5 standard deviations from the mean (red dots) are excluded from Figure 3. The reason for the large differences may be the inhomogeneous spatial distribution of aerosols.

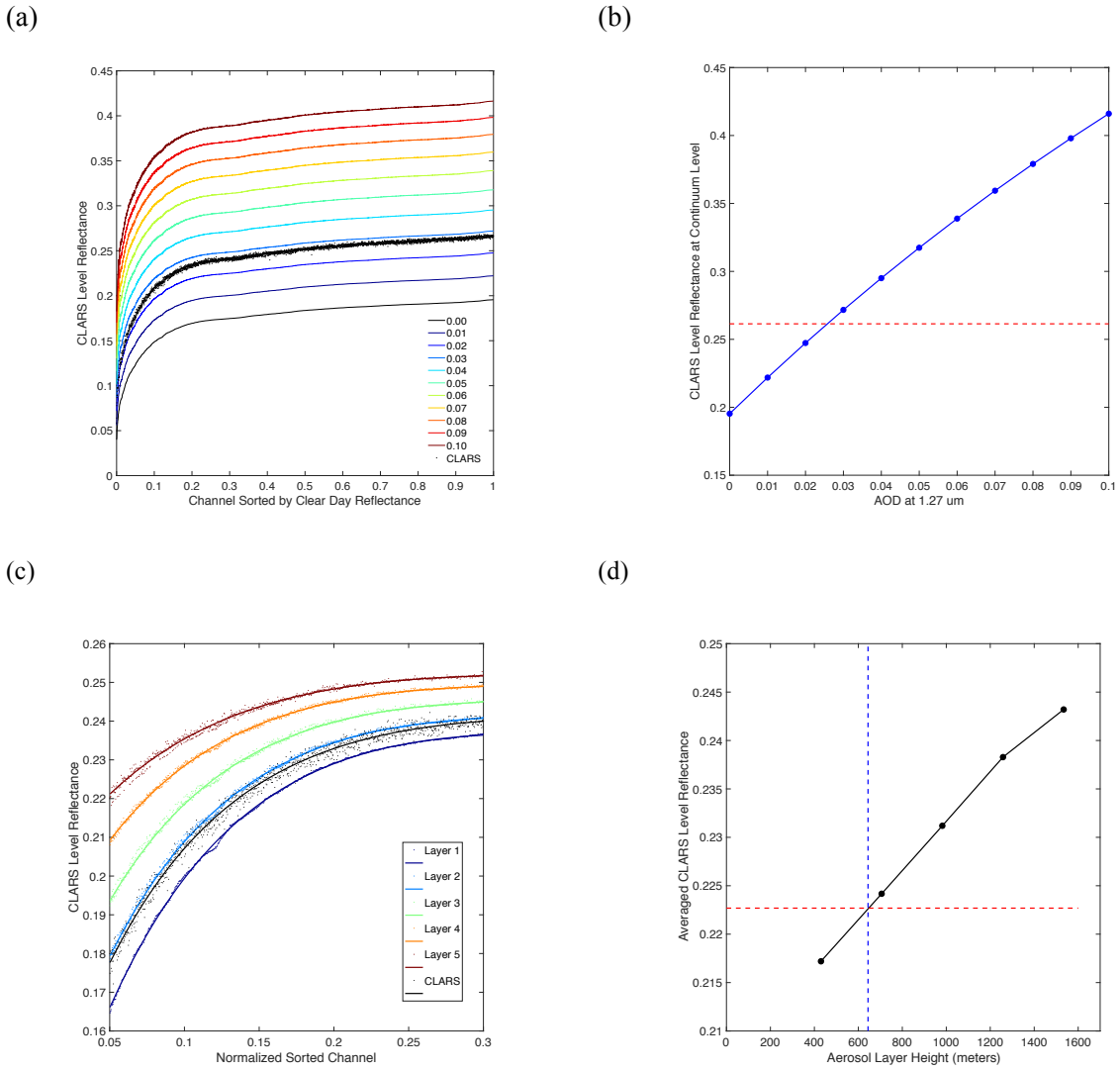

Figure S5. Examples of retrievals algorithms based on look up tables. The retrieval process can be separated into two steps. First, retrieve total AOD by constructing a look up table of simulated spectra using different values of total AOD, as shown in (a) and calculating the reflectance at the continuum level (the highest reflectance value), as shown in (b). In practice, to minimize uncertainty, the mean of the highest 50 reflectance values is used as the continuum level reflectance. Here, the aerosol is assumed to be vertically well-mixed. Second, retrieve the effective ALH after retrieving total AOD. The total AOD is uniformly partitioned into each of the five layers in the RT model, the simulated spectra are fitted using Equation (3) and finally compared with CLARS measurements, as shown in (c). In this analysis, the intermediate absorption band window (values between 0.05 and 0.3 of normalized sorted channel value), which shows the largest sensitivity to aerosol vertical structure, is used. Different metrics can be used to quantify the difference in reflectance between model simulations and measurements. Here, we use the mean value of reflectance over the intermediate absorption window calculated by averaging all CLARS level reflectance values, and build the look up table, as shown in (d). The dotted red line corresponds to the mean reflectance value of the CLARS measurement. The dotted blue line indicates the retrieved effective aerosol layer height.